The Impact of Aeroelastic Effects on the Controllability of Conventional Launch Vehicles

Mooij, Erwin; Gransden, Derek

Publication date
2016

Document Version
Final published version

Published in
Proceedings of the 67th International Astronautical Congress (IAC)

IAC–16–C2.3.14.x35230

The Impact of Aeroelastic Effects on the Controllability of Conventional Launch Vehicles

E. Mooij
Delft University of Technology, The Netherlands, E.Mooij@tudelft.nl

D.I. Gransden
Delft University of Technology, The Netherlands, D.I.Gransden@tudelft.nl

Sensor structural feedback and propellant sloshing have an adverse affect on the stability of conventional launch vehicles. Additionally, vehicle flight loads increase due to structural vibrations. However, in the conceptual design phase of a conventional launch vehicle, it is computationally expensive and undesirable to model the aeroelastic effects on its controllability, stability, and flight performance. Therefore, this paper focusses on the assumed-modes method of analysing aeroelastic effects on a slender-bodied conventional launch vehicle. The general model consists of the structural stiffness and mass properties, discretised over the length of the launcher; flight mechanics, which are simplified to only the pitch-plane equations; and engine swivel, acting as a control (thrust and moment) actuator. The structural representation and flight dynamics are combined in a state-space model with a simple PD controller to evaluate the stability and control of the system, without attempting to optimize for performance. The response to a step-command, with and without turbulence, is examined and compared for rigid, flexible modes, and flexible modes with sloshing effects. Flexible modes and sloshing effects have a destabilising influence, which, if coupled with non-optimal feedback signals, may result in excessive flight loads.

I. Introduction

Over time several specific examples of control problems occurring during flight tests of fighter aircraft have become apparent (Schwanz and Cerra, 1984). In each case, the cause of the problem could be characterised as inadequate modelling or other inappropriate treatment of the aero-elastic effects on the vehicle dynamics and/or the flight-control design. However, such problems are not restricted to just aircraft. Especially long and slender bodies such as (small) conventional launch systems may suffer from an unwanted coupling between the rigid body and its flexible modes. Therefore, this coupling should be analysed in detail, so it can be neglected if shown to be insignificant.

The stability of aeroelastic bodies such as missiles and launchers has been studied since the 1960s (Geissler, 1970; Lester and Collins, 1964; Meirovitch and Wesley, 1967) and invariably focussed on the interaction between rigid and flexible modes and the response to wind gust and turbulence, or the impact of aeroelasticity on control system stability margins, *e.g.*, the work done by Orr (2010). Even though the models for the flight dynamics are non-linear and derived with a Lagrangian approach, the analysis models are often linearised, see, for instance, Capri *et al.* (2006) and Orr *et al.* (2009). However, in some cases, the non-linear model is used to study the elastic dynamic effects on the trajectory (Li *et al.*, 2015). Aerodynamics models used vary from engineering methods, such as slender-body theory (ESDU, 1990), to linear quasi-steady piston theory (Noorian *et al*, 2016), or processed data from CFD analyses (Capri *et al.*, 2006; Li *et al.*, 2015). In many studies, though, details in vehicle and model data are not published, which make it hard to reproduce the analysis results.

The coupling effects between the rigid body and its flexible modes should not only be studied in the detailed design phase, but preferably at an early stage, such that information about stability and controllability can be fed into the structural-design process, and *vice versa*, information about aeroelasticity can be used in the analysis of flight performance, and the design and analysis of the control system. In the conceptual design phase, one wants to refrain from detailed finite element or CFD modelling, especially when many of the design choices on shape, layout and sub-systems have not yet been made. Therefore, the objective of this paper is to set up simplified models and an associated methodology to gain insight into the effect of aeroelasticity on launch vehicle stability, controllability, and controller performance.

Since large flexible structures are best modelled as distributed parameter systems, their motion is described by a system of coupled ordinary and partial differential equations, of which the latter are difficult to deal with both analytically and computationally. Therefore, approximate finite-dimensional equations of motion are usually used (Craig, 1981; Junkins and Kim, 1993). One of these methods is the assumed-modes method, where the deflection of continuous elastic structures is modelled by a finite series of space-dependent functions that are multiplied by specified time-dependent amplitude functions.

Therefore, in this paper, the assumed-modes method is applied to the conceptual design of a small launcher. The launcher is treated as a flexible beam with lumped masses to account for the subsystems and the fuel. A simplified mass-spring system is taken to model the mechanical aspects of fuel sloshing. The development of the simulation model will be discussed in detail, and the resulting model is analysed to establish the relevant bending modes. A multidisciplinary design approach integrating the models for trajectory, the structure, aerodynamics and control system is then employed to study the behaviour of a controlled, flexible launch vehicle in response to atmospheric turbulence.

Section 2 briefly reviews the assumed-modes method. Next, in Section 3, the structural design of the launcher is discussed, and how the modal shapes of the vehicle can be determined is summarised. Section 4 introduces the flight-dynamics model and shows how the external forces can be combined with the discrete structural model. As one needs a linearised system to do the control-system design and analysis, Section 5 provides an overview of the state-space model. The results of the analysis are given in Section 6, whereas Section 7 concludes this paper with some recommendations.

II. Background

To generate an N-degree-of-freedom approximate differential equation model for a continuous system, the displacement of the continuous system is expanded as a linear combination of N prescribed shape functions. In other words, the deformation $u(x,t)$ is approximated by

$$u(x,t) = \sum_{i=1}^{N} \phi_i(x)\eta_i(t) \qquad [1]$$

where x is the spatial coordinate, t is the time, $\phi_i(x)$ is the i^{th} assumed mode shape, $\eta_i(t)$ is the i^{th} generalised coordinate and N is the number of terms or modes that are included in the approximation.

To find expressions for the mode shapes, one can start by deriving the bending equation of motion for an undamped structure by applying the Principle of Virtual Work for a dynamic loading to a series of second-order elements, a so-called lumped-mass system. In matrix form, the equations of motion of such an (undamped) system is easily derived to be (Craig, 1981):

$$\mathbf{M}\ddot{\mathbf{u}} + \mathbf{K}\mathbf{u} = \mathbf{F} \qquad [2]$$

with $\mathbf{M}$ being the mass matrix, $\mathbf{K}$ the stiffness matrix, $\mathbf{u}$ the vector with displacements and $\mathbf{F}$ the forcing function. The homogeneous solution to Eq. [2] describing the free oscillations, also called the *in-vacuo* oscillations, can be written as

$$u_i(x,t) = U_i(x)e^{j\omega t} \qquad [3]$$

with U_i being the i^{th} displacement amplitude, ω the circular frequency of the oscillation, and j a complex variable being defined by j^2 = -1.

Solving for the N eigenfrequencies, Eq. [3] is substituted into Eq. [2] with $\mathbf{F} = \mathbf{0}$, yielding:

$$(-\omega^2\mathbf{M} + \mathbf{K})\mathbf{U} = \mathbf{0} \qquad [4]$$

The non-trivial solution is found by solving the eigenvalue problem

$$|-\omega^2\mathbf{M} + \mathbf{K}| = \mathbf{0} \qquad [5]$$

The corresponding eigenvectors can be selected as the shape functions $\phi_i(x)$, since they are usually the suitable space-dependent functions that satisfy not only all boundary conditions, but also the rigorous spatial differential equations.

Since the equations of motion Eq. [2] are coupled through the mass and the stiffness matrices, they can only be solved simultaneously. However, diagonalising $\mathbf{M}$ and $\mathbf{K}$ would simplify the solution, since each equation could then be solved independently. With the modal matrix $\mathbf{\Phi}$, consisting of the modal column vectors ϕ_i, then Eq. [1] can be written as

$$\mathbf{u}(x,t) = \mathbf{\Phi}(x)\boldsymbol{\eta}(t) \qquad [6]$$

Substituting the above equation into Eq. [2] and premultiplying each of the terms with $\mathbf{\Phi}^{\mathrm{T}}$ yields

$$\mathbf{\Phi}^{\mathrm{T}}\mathbf{M}\mathbf{\Phi}\,\ddot{\boldsymbol{\eta}} + \mathbf{\Phi}^{\mathrm{T}}\mathbf{K}\mathbf{\Phi}\,\boldsymbol{\eta} = \mathbf{\Phi}^{\mathrm{T}}\mathbf{F} \qquad [7]$$

Since the modal vectors are orthogonal the matrix multiplication with the mass and stiffness results in

diagonal matrices such that the equations are decoupled, *i.e.,*

$$\tilde{\mathbf{M}}\ddot{\boldsymbol{\eta}} + \tilde{\mathbf{K}}\boldsymbol{\eta} = \mathbf{Q} \quad [8]$$

where $\tilde{\mathbf{M}}$ is the modal mass matrix, $\tilde{\mathbf{K}}$ is the modal stiffness matrix, and $\mathbf{Q} = \boldsymbol{\Phi}^{\mathrm{T}}\mathbf{F}$ is the modal force vector. Finally, by using Rayleigh's Quotient, defined as (Craig, 1981)

$$\boldsymbol{\omega}^2 = \frac{\tilde{\mathbf{K}}}{\tilde{\mathbf{M}}} \quad [9]$$

The (decoupled) bending equations for an *undamped* system can be written as

$$\ddot{\boldsymbol{\eta}} + \boldsymbol{\omega}^2\boldsymbol{\eta} = \tilde{\mathbf{M}}^{-1}\mathbf{Q} \quad [10]$$

In the case there is (structural) damping, *e.g.,* due to internal friction in the material or at joints between components, Eq. [2] changes to

$$\mathbf{M}\ddot{\mathbf{u}} + \mathbf{C}\dot{\mathbf{u}} + \mathbf{K}\mathbf{u} = \mathbf{F} \quad [11]$$

where $\mathbf{C}$ is the damping matrix. It is common practice to assume that the structural damping is proportional to the so-called *critical damping*, which can be modelled as a fraction ζ_s. Following this approximation, Eq. [10] changes to

$$\ddot{\boldsymbol{\eta}} + 2\boldsymbol{\zeta}_s\boldsymbol{\omega}\dot{\boldsymbol{\eta}} + \boldsymbol{\omega}^2\boldsymbol{\eta} = \tilde{\mathbf{M}}^{-1}\mathbf{Q} \quad [12]$$

which is a decoupled system of differential equations. It is often assumed that there is zero damping in the structural analysis, *i.e.,* the natural modes may be computed for an undamped system (Geissler, 1970). However, when the response of the system is studied, *e.g.,* during control-system design, structural damping should be included in the model since it will have a noticeable effect on the results. Therefore, one can also write the *damped* deformation, indicated by the subscript d, as:

$$u_d(x,t) = \sum_{i=1}^{N} \phi_i(x)\eta_i(t) \quad [13]$$

To conclude the mathematical model, the rotation $\varphi_d(x,t)$ of (an element of) the structure is given by:

$$\varphi_d(x,t) = -\sum_{i=0}^{N} \sigma_i(x)\eta_i(t) \quad [14]$$

with $\sigma_i(x) = -\frac{\mathrm{d}\phi_i(x)}{\mathrm{d}x}$.

III. Structural Design

Modelling a flexible structure in the feasibility phase of the design should be as simple as possible while still including a sufficient level of detail, which results in structural characteristics of the vehicle that will give a reasonable approximation of the final vehicle. It is common practice to use a beam analogy for modelling a conventional launcher. Geissler (1970) states that it is sufficient to use about 40 nodes to derive the first four bending modes with reasonable accuracy. The shape functions can be defined by the nodal displacement eigenvectors, which means that they have also a dimension of about 40, albeit with six components per entry (three translations and three rotations). Looking at the bending motion in the pitch plane only, one only requires two components, *i.e.,* the translation in the Z-direction (inducing a change in (local) angle of attack) and a (pitch) rotation about the Y-axis. The other four degrees of freedom are constrained.

The launcher will be modelled as a beam with lumped masses that represent the launcher's subsystems, such that the in-vacuo eigenfrequencies can be approximated. The two-stage PacAstro launcher for small payloads up to 350 kg has been selected for its availability of some geometrical and structural data*. The PacAstro is divided into a number of sections, such as *aft skirt*, *LOX tanks*, *etc.*, see Table 1 for an overview of dimensions and associated masses. Each of these sections is, in fact, a monocoque structure with wall thickness t; although, here simple beam elements are used in the model. These beam elements represent the same cross-sectional area and inertia properties. The modelling of the fuel and oxidiser tanks when they are not completely full is divided into two parts. It is assumed that all fuel (or oxidiser) is at the lower part of the tank, such that the tank can actually be modelled as two separate tanks, *i.e.,* one empty and one full. Table 2 lists the applied materials. Note that for a section k, the first node is equal to the last node of section $k-1$, whereas the last node is equal to the first node of section $k+1$. The total number of nodes is 43.

The remainder of this paper examines at the stability of the PacAstro at the point of maximum dynamic pressure. From a trajectory analysis, this point

*PacAstro was a US transportation service company, formed in 1990, to provide low-cost transportation of small satellites to Low Earth Orbit for approximately $5 million per launch using proven technology (Fleeter *et al.*, 1992). Unfortunately, the launcher never came to operation despite several engine tests and three launch contracts, due to the lack of development funding. The company ceased to be in 1997.

Table 1: Simplified dimensional model of PacAstro

section	x (m)	dx (m)	t (mm)	m (kg)
aft skirt 1	0.000	2.824	0.687	30.5
engine 1	2.200	-	-	360.0
fuel tank 1	2.824	3.446	2.64	226.2
intertank 1	6.270	2.110	3.10	102.7
LOX tank 1	8.380	6.220	3.46	535.3
interstage	14.600	3.310	2.59	134.6
fuel tank 2	17.910	0.389	1.65	16.0
intertank 2	18.299	1.570	2.24	55.2
LOX tank 2	19.869	1.090	1.79	48.6
forward skirt 2	20.959	1.010	1.60	25.4
fairing cylinder	21.969	1.000	1.46	22.7
fairing frustrum	22.969	2.800	1.23	53.5
payload	22.969	-	-	225.0
frustrum end	25.769	-	-	

Table 2: Material types and properties

nr	material	σ_{yield} (MPa)	E (N/m^2)	ρ (kg/m^3)
1	Al 7075 T6	441	$7.24{\cdot}10^{10}$	2740
2	Al 2024 T4	290	$7.38{\cdot}10^{10}$	2710
3	Ti 6Al 4V	986	$1.13{\cdot}10^{11}$	4430

has been identified to occur at $t = 63$ s. For this condition, the remaining fuel for the first stage is $m_{f,1} = 3{,}614.7$ kg, with the assumed free surface located at $x_{f,1} = 3.69$ m (measured from the base of the launcher). The free surface of the oxidiser is located at $x_{o,1} = 9.94$ m, with an equivalent mass of 8,675.1 kg. Similarly, for the second stage, the free surface is located at $x_{f,2} = 18.1$ m ($m_{f,2} = 1{,}830$ kg) for the fuel, and at $x_{o,2} = 20.41$ m ($m_{o,2} = 4{,}369$ kg) for the oxidiser. It is noted that the stiffness properties of the fuel and oxidiser can be lowered compared to their respective tank values to account for sloshing; although this may not the best way to take the effect into account.

For the time point under consideration, the total mass of the launcher as described above is $m = 20{,}762$ kg, with a centre of mass location of $x_{cm} = 12.09$ m, and a pitch-moment of inertia of $I_{yy} = 8.024{\cdot}10^5$ kgm^2. In Fig. 1, the mass and stiffness properties of the modelled launcher are shown as a function of the axial location. Calculating (with NASTRAN) the normalised bending modes for this configuration gives the first four modes as shown in Fig. 2. In Table 3, the variation with time of the first two modes is listed.

If the fuel and oxidiser can move freely, they will affect the eigenmodes of the elastic vehicles. Modelling

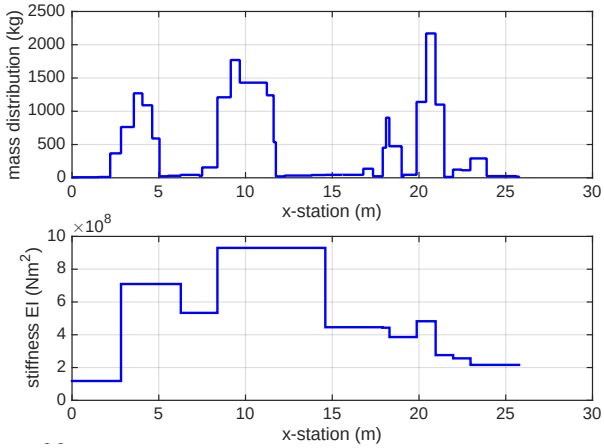

Fig. 1: Discretised launcher model ($t = 63$ s)

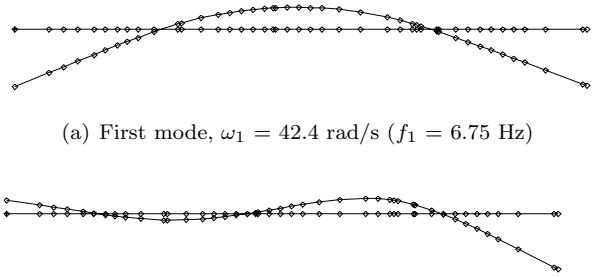

(a) First mode, $\omega_1 = 42.4$ rad/s ($f_1 = 6.75$ Hz)

(b) Second mode, $\omega_2 = 126.7$ rad/s ($f_2 = 20.16$ Hz)

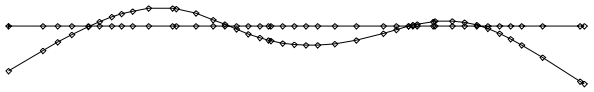

(c) Third mode, $\omega_3 = 281.6$ rad/s ($f_3 = 44.81$ Hz)

(d) Fourth mode, $\omega_4 = 408.7$ rad/s ($f_4 = 65.04$ Hz)

Fig. 2: First four normalised bending modes of the PacAstro ($t = 63$ s)

Table 3: Structural natural frequencies along trajectory

time (s)	1^{st} mode (rad/s)	2^{nd} mode (rad/s)
35	37.6 (5.98 Hz)	122.4 (19.48 Hz)
63	42.4 (6.75 Hz)	126.7 (20.17 Hz)
126	77.9 (12.40 Hz)	167.2 (26.61 Hz)

Table 4: Eigenfrequencies at $t = 63$ s

structural mode	no sloshing ω_i (rad/s)	sloshing ω_i (rad/s)
1	–	7.0
2	–	7.5
3	42.4	45.7
4	126.7	127.6
5	281.6	329.4
6	408.7	426.0

sloshing is not a trivial matter, and one can find a lot of literature on theoretical and practical aspects on the subject, *e.g.,* that by U.S. Army (1969) and Ibrahim (2005). A simple approach may be to model the moving liquid as one or more (damped) mass-spring systems (Ebrahimian, 2014), damped pendulum(s) (Nichkawde *et al.*, 2004), or extract data from a detailed CFD analysis (Yang and Peugeot, 2014). However, finding the proper stiffness and damping parameters depends a great deal on the liquid properties, as well as the shape of the tanks, the filling grade and the internal structure of the tanks, *e.g.,* whether there are damping baffles present or not.

In light of the simplified modelling and still being able to take any effect of sloshing into account, one can lower the stiffness of those portions of the beam model that include the fuel and oxidiser, albeit only in partially filled tanks. In Table 4, the eigenfrequencies of the first four bending modes and two sloshing modes (two tanks) are listed. The sloshing modes approach rigid-body modes, and the bending modes are hardly affected by the sloshing, *i.e.,* the modes are well separated.

The engine of the first stage can be swivelled, and as such can act as a control actuator: the engine does not only produce a thrust force, but also a moment. It is common to consider the nozzle motion to be instantaneous in rigid-body simulations. Swivelling will thus have no effect on the eigenmotion of the (rigid) system. However, when a flexible launch system is studied, this assumption may be invalid, and one has to make sure that the natural frequency of the engine is well separated from (at least) the first bending mode. Therefore, the engine is considered to be an electro-hydraulic servo system that can be approximated by a third-order system, of which the Laplace form is given by (Rolland Collette, 1967):

$$\left(s^3 + 2\zeta_e\omega_e s^2 + \omega_e^2 s + K_e\omega_e^2\right)\varepsilon_T = K_e\omega_e^2\varepsilon_{T,c} \quad [15]$$

where the load torque feedback terms have been neglected; these terms include all inertia-load torques due to the accelerations of the rigid and flexible modes, but are small compared to the remaining terms. In Eq. [15], ω_e and ζ_e are the natural frequency and damping of the engine dynamics. The gain K_e is an amplification factor that improves the response (time), but does have a tendency to *lower* the natural frequency of the engine modes. The two thrust-elevation angles ε_T and $\varepsilon_{T,c}$ are the actual and commanded value, respectively. Equation [15] will be converted into state-space form in Section 5 and linked with the flight model.

IV. Flight Model

The current paper focusses on the pitch-plane motion of a launcher at a particular point in its trajectory, *i.e.,* at $t = 63$ s. Next, one must link the (flexible) structural model with the flight-dynamics model, and establish a relation between the deformed structure and the external forces and moments. In Fig. 3, the geometry of the deformed launcher has been depicted. For the sake of the analysis we assume a non-rotating flat Earth, where the launcher has a velocity $V = u_0 = 493.07$ m/s and a pitch angle $\theta_0 = 61.7°$ with respect to the inertial plane. The related external forces acting upon the system are the thrust, T, the normal force, N, and the weight, W. The thrust orientation is defined by the swivel angle ε_T, and the magnitude of N is defined by the angle of attack α at a given Mach number, $M = 1.85$. In general, the normal deformation with respect to the undeformed elastic axis is indicated by $u_d(x,t)$, and the corresponding rotation is defined by $\varphi(x,t)$.

The current study will focus on the pitch-plane motion and explores only small deviations from the

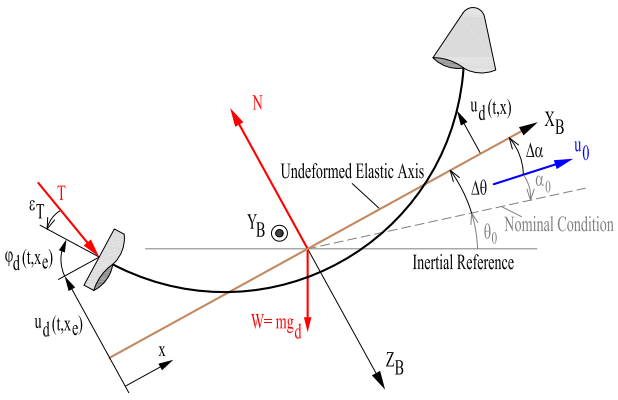

Fig. 3: Flexible vehicle definitions

vertical trajectory. The rigid-body equations of motion are obtained by linearising the non-linear equations of motion as given by (Etkin and Reid, 1996):

$$\begin{aligned}\Delta\dot{u} &= \frac{\Delta X_B}{m} - g_d \cos\theta_0 \Delta\theta \\ \Delta\dot{w} &= \Delta q u_0 + \frac{\Delta Z_B}{m} - g_d \sin\theta_0 \Delta\theta \\ \Delta\dot{q} &= \frac{\Delta M_y}{I_{yy}}\end{aligned} \qquad [16]$$

Furthermore, because the angle of attack can replace the (small) vertical velocity through the relation

$$\Delta\alpha = \frac{\Delta w}{u_0} \qquad \Rightarrow \qquad \Delta\dot{\alpha} = \frac{\Delta\dot{w}}{u_0} \qquad [17]$$

one obtains for the pitch-plane equations, for a single trajectory point (constant position and velocity) and dropping the Δ-notation:

$$\dot{\alpha} = q + \frac{Z_B}{m u_0} - \frac{g_d \sin\theta_0 \theta}{u_0} \qquad [18]$$

$$\dot{q} = \frac{M_y}{I_{yy}} \qquad [19]$$

with the (rigid-body) force and moment given by (see Fig. 3)

$$Z_B = F_{A,z} + F_{T,z} = -N + T\sin\varepsilon_T \qquad [20]$$

$$M_y = M_{A,y} + M_{T,z} = \mathcal{M} + L_e T \sin\varepsilon_T \qquad [21]$$

where $\mathcal{M}$ is the aerodynamic pitch moment, and the thrust-moment arm $L_e = x_{cm} - x_e$. Here, x_{cm} and x_e are the axial locations of the centre of mass and engine (thrust point), respectively. The flight-point under consideration is at $L_e = 9.8034$ m.

In the above setup, the engine dynamics are uncoupled from the rigid-body equations. However, the effects resulting from the movement of the engine (swivelling) can have a considerable effect upon the dynamics of the total vehicle, this dynamic mode has to be coupled with the equations derived so far. This can easily be done by introducing the forces and moments the engine exerts on the vehicle. Due to the angular acceleration of the engine around its gimbal point, a force on the gimbal point ($x_g = 2.2$ m) in the direction of a positive ε_T is introduced. A reaction force is then applied on the vehicle. For small thrust angles, this force may be approximated by

$$F_{z_e} = m_e \Delta L_{cm,e} \ddot{\varepsilon}_T \qquad [22]$$

where m_e is the mass of the engine and $\Delta L_{cm,e}$ is the distance from gimbal point to centre of mass of the engine. This force also contributes to a pitch moment. The moment due to engine swivelling further includes an external torque applied to the engine by the servo actuator, $M_{e,servo} = I_e \ddot{\varepsilon}_T$, with I_e being the engine moment of inertia. Combined, the total moment that originates from engine swivelling is then given by:

$$M_{y_e} = \left(L_e m_e \Delta L_{cm,e} + I_e\right) \ddot{\varepsilon}_T \qquad [23]$$

Including the loads given by Eqs. [22] and [23] will also account for the possible occurrence of the *tail-wags-dog*. This effect occurs when the inertia force resulting from gimballing the engine cancels the lateral component of the thrust due to the deflection of the engine. For this study, the following representative data have been used: $m_e = 225$ kg, $I_e = 300$ kg m^2 and $\Delta L_{cm,e} = 0.7$ m.

The behaviour of a flexible vehicle, where the structure will also deform due to the forces and moments as discussed previously, requires one to incorporate the bending equations of motion and introduce the relevant coupling terms in the model. The system of equations is derived earlier, Eq. [12], so now the focus is on the coupling with the external loads.

For the short-period symmetric motion that is the topic of interest, the quasi-steady rigid-body aerodynamic force and moment depend primarily on the normal velocity, w, and the pitch rate, $q = \dot{\theta}$ (Lester and Collins, 1964; Nielsen, 1960). The dependence on higher powers of the angle of attack and possibly other quantities is very small, so they can be ignored for this kind of study (Seifert and Brown, 1961). Therefore, for a single point in the trajectory (constant Mach number) the normal force and pitch moment are given as $f(\alpha, q)$. The dependency on q is easily understood. A pitch rate originates from the fact that the launcher follows a curved flight path. The pitch rate induces a normal-velocity distribution along the vehicle, which results in an increase of local angle of attack (when multiplied with the distance from the centre of mass, the point of rotation). Additionally, the situation is further complicated, due to the deformation of the launcher, such that the angle between the X-axis and the disturbed velocity vector varies along the vehicle. This results in an additional dependency on the generalised coordinates and their time derivatives.

The rigid-body aerodynamic model is based on a blunted-cone forebody with cylindrical extension and no boat-tailing. The method applied is one based on slender-body theory and described by ESDU (1990). In essence, it assumes that both the normal-force and the pitching-moment curve of such configura-

tions can be evaluated as the sum of three components. The major contribution comes from the (inviscid) flow over the forebody and generates a loading that may also extend onto the cylindrical part. The second and third components originate from the development of a viscous boundary layer (fully turbulent) along the length of the body. The boundary layer represents a displacement thickness that modifies the flow. The other boundary-layer contribution arises from the frictional force acting over the surface of the body. Numerical details about each of these three components for Mach numbers up to $M_\infty = 5$ and different ratios of length-to-diameter, as well as a range of Reynolds numbers, is provided by ESDU (1990).

For slender bodies of revolution with a cone-shaped forebody and cylindrical afterbody, the distribution on the forebody constitutes the larger part of the total normal force. Lester and Collins (1964) assume a linear lift build-up over the forebody and an exponential decay over the afterbody. This distribution is validated by various experiments, see, for instance, the book by Nielsen (1960), and will qualitatively closely resemble the actual normal-force distribution on a small launch vehicle. To calculate $C_{N_\alpha}(x)$, it is assumed that $C^*_{N_\alpha}$ and $C^*_{m_\alpha}$ are available for the flight condition under consideration, calculated with the algorithm provided by ESDU (1990). The distributed load should of course lead to the same total slope coefficient. This can be achieved with:

$$C^*_{N_\alpha} = c_1 \int_0^{L_b} c_2^{\frac{x}{L_b}} \mathrm{d}x + c_1 \frac{c_2}{L_n} \int_{L_b}^{L_{tot}} (L_{tot} - x)\mathrm{d}x \qquad [24]$$

$$\begin{aligned} d_{ref} \cdot C^*_{m_\alpha} = c_1 \int_0^{L_b} c_2^{\frac{x}{L_b}} (x - L_b)\mathrm{d}x \\ + c_1 \frac{c_2}{L_n} \int_{L_b}^{L_{tot}} (L_{tot} - x)(x - L_b)\mathrm{d}x \end{aligned} \qquad [25]$$

where the total vehicle length, L_{tot}, is the sum of the body length, L_b, and nose length, L_n, so $L_{tot} = L_b + L_n$, and d_{ref} is a reference length (typically the vehicle diameter). The first part on the right-hand side of Eqs. [24] and [25] represent the exponential decay of the afterbody, whereas the second part gives the linear increase of the nose-region of the vehicle. The coefficients c_1 and c_2, defining the magnitude of the distribution, can be determined iteratively. For $M = 1.85$, it was found that $C^*_{N_\alpha} = 3.7954$ and $C^*_{m_\alpha} = 29.303$ rad^{-1}, which yielded $c_1 = 4.6{\cdot}10^{-3}$ and $c_2 = 13.622$. As an example, the corresponding distributed normal load is shown in Fig. 4.

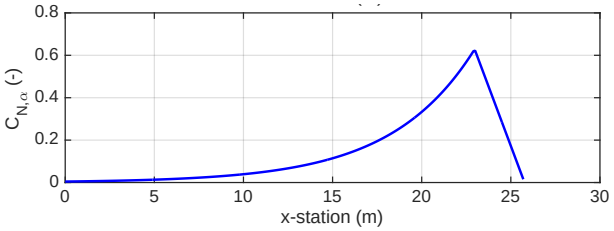

Fig. 4: Normal load distribution

If, for a location x_j, the local coefficients are given by $C^j_{N_\alpha}$ and $C^j_{m_\alpha}$, then, with n axial stations, it follows for the rigid-body coefficients:

$$C_{N_\alpha} = \sum_{j=0}^{n} C^j_{N_\alpha} \qquad C_{m_\alpha} = \sum_{j=0}^{n} C^j_{m_\alpha} \qquad [26]$$

$$\begin{aligned} C_{N_q} &= -\frac{1}{u_0} \sum_{j=0}^{n} C^j_{N_\alpha} \cdot \Delta x_{cm,j} \\ C_{m_q} &= -\frac{1}{u_0} \sum_{j=0}^{n} C^j_{m_\alpha} \cdot \Delta x_{cm,j} \end{aligned} \qquad [27]$$

where $\Delta x_{cm,j} = x_j - x_{cm}$.

Summarising, and considering the perturbations around an otherwise nominal state, the normal (aerodynamic) force can thus be written as:

$$\begin{aligned} F_{A,z} = \bar{q} S_{ref} \int_0^{L_{tot}} \frac{\partial C_N}{\partial \alpha}(x)\alpha(x)\mathrm{d}x \\ - \bar{q} S_{ref} \frac{q}{u_0} \int_0^{L_{tot}} \frac{\partial C_N}{\partial \alpha}\alpha(x)(x_{cm} - x)\mathrm{d}x \\ + \sum_{i=1}^{N} \frac{\partial F_{Z,A}}{\partial \eta_i}\eta_i + \sum_{i=1}^{N} \frac{\partial F_{Z,A}}{\partial \dot{\eta}_i}\dot{\eta}_i \end{aligned} \qquad [28]$$

where $\bar{q} = \frac{1}{2}\rho u_0^2$ is the dynamic pressure and S_{ref} is the reference area ($S_{ref} = 2.63$ m^2). The dependence of the aerodynamic force on the generalised coordinates has an effect similar to the rigid-body angle of attack. The velocity of η_i has an effect similar to the rigid-body pitch rate.

The individual partials and integral terms can all be written as aerodynamic coefficients (Lester and Collins, 1964). When defining $C'_{N_\alpha} = \frac{\partial C_N}{\partial \alpha}(x)$, with the prime indicating a geometric dependency, then:

$$C_{N_\alpha} = \int_0^{L_{tot}} C'_{N_\alpha}\mathrm{d}x \qquad [29]$$

$$C_{N_q} = -\frac{1}{u_0}\int_0^{L_{tot}} C'_{N_\alpha}(x - x_{cm})\mathrm{d}x \qquad [30]$$

$$C_{N_{\eta_i}} = \int_0^{L_{tot}} C'_{N_\alpha}\,\sigma_i(x)\mathrm{d}x \qquad [31]$$

$$C_{N_{\dot{\eta}_i}} = -\frac{1}{u_0}\int_0^{L_{tot}} C'_{N_\alpha}\,\phi_i(x)\mathrm{d}x \qquad [32]$$

with σ_i and ϕ_i being the (position-dependent) values of the eigenvector of the i^{th} (bending) mode, *i.e.,* the rotation and translation component, respectively. The moment coefficients C_{m_α}, C_{m_q}, $C_{m_{\eta_i}}$ and $C_{m_{\dot{\eta}_i}}$ have the same form, only the integrand is multiplied with $x - x_{cm}$, which represents the aerodynamic moment arm as a function of x.

The total force and moment are thus written as:

$$F_{A,z} = -\Big(C_{N_\alpha}\alpha + C_{N_q}q + \sum_{i=1}^{N} C_{N_{\eta_i}}\eta_i + \sum_{i=1}^{N} C_{N_{\dot{\eta}_i}}\dot{\eta}_i\Big)\bar{q}S_{ref} \qquad [33]$$

$$M_{A,y} = \Big(C_{m_\alpha}\alpha + C_{m_q}q + \sum_{i=1}^{N} C_{m_{\eta_i}}\eta_i + \sum_{i=1}^{N} C_{m_{\dot{\eta}_i}}\dot{\eta}_i\Big)\bar{q}S_{ref}d_{ref} \qquad [34]$$

with the reference length, d_{ref}, assumed to be 1 m.

As can be seen in Fig. 3, the deflection of the launcher will rotate the engine such that the thrust direction changes. This has, of course, an impact on the contribution to Z_B and M_y. The additional thrust contribution is:

$$\Delta F_{T,z} = -T\sum_{i=1}^{N}\eta_i\sigma_i(x_e) \qquad [35]$$

where $\sigma_j(x_e)$ is the rotational component of the eigenvector of mode j at the engine location. Similarly, the additional thrust moment is

$$\Delta M_{T,y} = -L_eT\sum_{i=1}^{N}\eta_i\sigma_i(x_e) - T\sum_{i=1}^{N}\eta_i\phi_i(x_e) \qquad [36]$$

The first component follows from the force contribution, Eq. [35], whereas the second component originates from the (translational) elastic deflection.

In summary, for a flexible body the force, Z_B, consists of the components given by Eqs. [20], [22], [33] and [35], whereas the moment, M_y, is defined by Eqs. [21], [23], [34] and [36]. Finally, the gravitational load must be distributed over the axial stations and its effect included in the bending equations [12]†. The change in shape affects each bending mode differently; the contribution to the generalised force for bending mode i is simply:

$$F_{g,i} = -g_d\sin\theta_0\int_0^{L_{tot}}\phi_i(x)m(x)\mathrm{d}x \qquad [37]$$

V. State-Space Model

The mathematical model that has been set up must lead to a state-space model for the error dynamics that can be used for the stability and control analysis. The task at hand is relatively simple, as the models in the previous sections are linear models, *i.e.,* the rigid-body states are small deviations around the nominal trajectory or the control-system design point, the engine dynamics hold for small swivel angles, and the bending equations are, as defined, linear.

In its general form, the system equation of the state-space model for the error dynamics is given by

$$\dot{\mathbf{x}} = \mathbf{A}\mathbf{x} + \mathbf{B}\mathbf{u} \qquad [38]$$

with $\mathbf{A}$ and $\mathbf{B}$ being the the system and control matrix, respectively. Due to the different groups of state variables, it is sensible to decompose these matrices to keep track of where the coefficients have come from. Three indices suffice to distinguish these groups, *i.e.,*

1. R for the rigid-body states α, θ and q;
2. E for the engine states $\ddot{\varepsilon}_T$, $\dot{\varepsilon}_T$ and ε_T. These states originate from the assumption that the engine is modelled as an electro-hydraulic servo system, represented by a third-order transfer function;
3. F for the flexible-body states $\dot{\eta}_i$ and η_i for mode i. The total number of states in this group depends on how many bending modes N are taken into account. In case sloshing is considered, modes with a lower frequency are introduced, which means that more bending modes may have an effect on the motion.

$$\mathbf{A} = \begin{bmatrix} \mathbf{A_{RR}} & \mathbf{A_{RE}} & \mathbf{A_{RF}} \\ \mathbf{A_{ER}} & \mathbf{A_{EE}} & \mathbf{A_{EF}} \\ \mathbf{A_{FR}} & \mathbf{A_{FE}} & \mathbf{A_{FF}} \end{bmatrix} \qquad [39]$$

†When one would derive the bending equations of motion starting with the Lagrange equation, the contribution of gravity would be included in the potential energy.

$$\mathbf{B} = \begin{pmatrix} \mathbf{B_R} \\ \mathbf{B_E} \\ \mathbf{B_F} \end{pmatrix} \quad [40]$$

The state vector, $\mathbf{x}$, is thus given by

$$\mathbf{x}^{\mathrm{T}} = (\alpha\, \theta\, q\, \ddot{\varepsilon}_T\, \dot{\varepsilon}_T\, \varepsilon_T\, \dot{\eta}_1\, \eta_1 \ldots \dot{\eta}_N\, \eta_N)^{\mathrm{T}}$$

The only control is the commanded swivel angle, so $u = \varepsilon_{T,c}$.

In the definition of $\mathbf{A}$, $\mathbf{A_{ER}} = \mathbf{A_{EF}} = \mathbf{0}$. The non-zero matrices are defined as follows:

$$\mathbf{A_{RR}} = \begin{bmatrix} -\frac{C_{N_\alpha}\bar{q}S_{ref}}{mu_0} & -\frac{g_d \sin\theta_0}{u_0} & \frac{C_{N_q}\bar{q}S_{ref}}{mu_0} + 1 \\ 0 & 0 & 1 \\ \frac{C_{m_\alpha}\bar{q}S_{ref}}{I_{yy}} & 0 & \frac{C_{m_q}\bar{q}S_{ref}}{I_{yy}} \end{bmatrix} \quad [41]$$

$$\mathbf{A_{RE}} = \begin{bmatrix} \frac{m_e \Delta L_e}{mu_0} & 0 & \frac{T}{mu_0} \\ 0 & 0 & 0 \\ \frac{m_e L_e \Delta L_e + I_e}{I_{yy}} & 0 & \frac{L_e T}{I_{yy}} \end{bmatrix} \quad [42]$$

$$\mathbf{A_{RF}} = \begin{bmatrix} a_{\alpha,\dot{\eta}_1} & a_{\alpha,\eta_1} & \ldots & a_{\alpha,\dot{\eta}_N} & a_{\alpha,\eta_N} \\ 0 & 0 & \ldots & 0 & 0 \\ a_{q,\dot{\eta}_1} & a_{q,\eta_1} & \ldots & a_{q,\dot{\eta}_N} & a_{q,\eta_N} \end{bmatrix} \quad [43]$$

with, for $i = 1, \ldots, N$:

$$a_{\alpha,\dot{\eta}_i} = -C_{N_{\dot{\eta}_i}}\bar{q}S_{ref}$$

$$a_{\alpha,\eta_i} = -\frac{C_{N_{\eta_i}}\bar{q}S_{ref} - T\sigma_i(x_e)}{mu_0}$$

$$a_{q,\dot{\eta}_i} = \frac{C_{q,\eta_i}\bar{q}S_{ref}d_{ref}}{I_{yy}}$$

$$a_{q,\eta_i} = \frac{C_{m_{\eta_i}}\bar{q}S_{ref}d_{ref} - L_e T\sigma_i(x_e) - T\phi_i(x_e)}{I_{yy}}$$

$$\mathbf{A_{EE}} = \begin{bmatrix} -2\zeta_e\omega_e & -\omega_e^2 & -K_e\omega_e^2 \\ 1 & 0 & 0 \\ 0 & 1 & 0 \end{bmatrix} \quad [44]$$

For the current study, $K_e = 15$, $\omega_e = 50$ rad/s, $\zeta_e = 0.7$. As mentioned before, selecting $K_e > 1$ will lower the eigenfrequency of the engine dynamics, as is shown in the next section.

Each bending motion depends on the generalised force for that specific motion. This generalised force is found by multiplying all the external loads with the eigenvector of that mode. The external loads are again a function of the bending motion and the position along the vehicle. Note that the subscripts i and j below both indicate a flexible mode, up to the maximum of N.

$$\mathbf{A_{FR}} = \begin{bmatrix} a_{\dot{\eta}_1,\alpha} & a_{\dot{\eta}_1,\theta} & a_{\dot{\eta}_1,q} \\ 0 & 0 & 0 \\ \vdots & \vdots & \vdots \\ a_{\dot{\eta}_N,\alpha} & a_{\dot{\eta}_N,\theta} & a_{\dot{\eta}_N,q} \\ 0 & 0 & 0 \end{bmatrix} \quad [45]$$

with

$$a_{\dot{\eta}_i,\alpha} = -\bar{q}S_{ref} \int_0^{L_{tot}} C'_{N_\alpha}\phi_i(x)\mathrm{d}x \quad [46]$$

$$a_{\dot{\eta}_i,\theta} = -g_d \sin\theta_0 \int_0^{L_{tot}} \phi_i(x)m(x)\mathrm{d}x \quad [47]$$

$$a_{\dot{\eta}_i,q} = -\frac{\bar{q}S_{ref}}{u_0} \int_0^{L_{tot}} (x - x_{cm})C'_{N_\alpha}\phi_i(x)\mathrm{d}x \quad [48]$$

$$\mathbf{A_{FE}} = \begin{bmatrix} a_{\dot{\eta}_1,\ddot{\varepsilon}_T} & 0 & a_{\dot{\eta}_1,\varepsilon_T} \\ 0 & 0 & 0 \\ \vdots & \vdots & \vdots \\ a_{\dot{\eta}_N,\ddot{\varepsilon}_T} & 0 & a_{\dot{\eta}_N,\varepsilon_T} \\ 0 & 0 & 0 \end{bmatrix} \quad [49]$$

with

$$a_{\dot{\eta}_i,\ddot{\varepsilon}_T} = m_e \Delta L_{cm,e}\phi_i(x_e) + I_e\sigma_i(x_e)$$

$$a_{\dot{\eta}_i,\varepsilon_T} = T\phi_i(x_e)$$

$$\mathbf{A_{FF}} = \begin{bmatrix} a_{\dot{\eta}_1,\dot{\eta}_1} & a_{\dot{\eta}_1,\eta_1} & \ldots & a_{\dot{\eta}_1,\dot{\eta}_N} & a_{\dot{\eta}_1,\eta_N} \\ a_{\eta_1,\dot{\eta}_1} & a_{\eta_1,\eta_1} & \ldots & a_{\eta_1,\dot{\eta}_N} & a_{\eta_1,\eta_N} \\ \vdots & \vdots & \vdots & \vdots & \vdots \\ a_{\dot{\eta}_N,\dot{\eta}_1} & a_{\dot{\eta}_N,\eta_1} & \ldots & a_{\dot{\eta}_N,\dot{\eta}_N} & a_{\dot{\eta}_N,\eta_N} \\ a_{\eta_N,\dot{\eta}_1} & a_{\eta_N,\eta_1} & \ldots & a_{\eta_N,\dot{\eta}_N} & a_{\eta_N,\eta_N} \end{bmatrix} \quad [50]$$

with, for $i \neq j$:

$$a_{\dot{\eta}_i,\dot{\eta}_j} = -\frac{\bar{q}S_{ref}}{u_0} \int_0^{L_{tot}} \phi_i(x)C'_{N_\alpha}\phi_j(x)\mathrm{d}x$$

$$a_{\dot{\eta}_i,\eta_j} = -\bar{q}S_{ref} \int_0^{L_{tot}} \phi_i(x)C'_{N_\alpha}\sigma_j(x)\mathrm{d}x - T\phi_i(x_e)\sigma_j(x_e)$$

$$a_{\eta_i,\dot{\eta}_j} = a_{\eta_i,\eta_j} = 0$$

and for $i = j$

$$a_{\dot{\eta}_i,\dot{\eta}_i} = a_{\dot{\eta}_i,\dot{\eta}_i} - 2\zeta_i\omega_i^2$$

$$a_{\dot{\eta}_i,\eta_i} = a_{\dot{\eta}_i,\eta_i} - \omega_i^2$$
$$a_{\eta_i,\dot{\eta}_i} = 1$$
$$a_{\eta_i,\eta_i} = 0$$

Note: the structural damping ζ_i has not been determined according to any design. Vibration tests show that the structural damping is at most a few percent of the critical damping. Therefore, a structural damping of $\zeta_i = \zeta_s = 0.015$ is used in this study, which is a spacecraft industry standard (Foist *et al.*, 2004).

Lastly, to complete the model description, the components of $\mathbf{B}$ are necessary:

$$\mathbf{B_R} = \mathbf{B_F} = \mathbf{0} \quad [51]$$

and

$$\mathbf{B_E} = \begin{pmatrix} K_e\omega_e^2 \\ 0 \\ 0 \end{pmatrix} \quad [52]$$

VI. Results

Stability and Control Analysis

As a measure of the stability of the launch vehicle, the gain and phase margin of the system can be investigated. The gain margin is the factor by which the overall system gain can be increased before instability occurs. Both the rigid body control mode and gain stabilised bending modes require a gain margin of about 6dB. The phase margin is the additional phase lag that the vehicle can tolerate without becoming unstable. The rigid-body control mode requires a phase margin of 30° and phase-stabilised bending modes should have a margin of 40° (Seifert and Brown, 1961).

The stability and control analysis will be treated in several steps. To begin, the eigenvalues of the rigid body ($\mathbf{A_{RR}}$) are all real, of which two are unstable: λ_1 = -2.1288, λ_2 = 1.9811, and λ_3 = 0.0175. The two larger eigenvalues are associated with the rigid-body rotation around the centre of mass, and with an unstable mode the need for a control system is obvious. The small, unstable mode is associated with a drift of the flight path in response to wind. This drift is quite small in comparison with the other unstable mode, so it will not cause any serious problems. Figure 5 shows the eigenvalues of the complete system, including engine dynamics and bending modes.

To stabilise the rigid body a simple PD controller is implemented, as the goal of this study is not to design the best control system possible. According

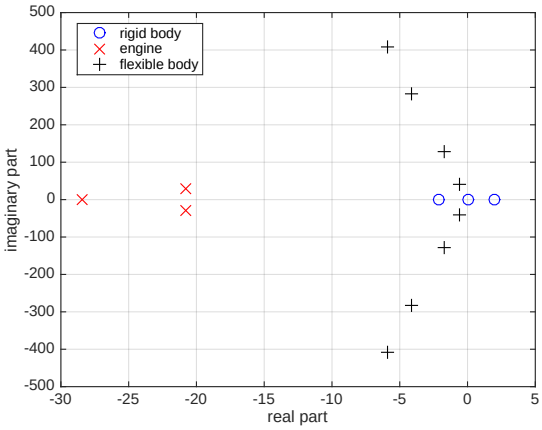

Fig. 5: Uncoupled, open-loop eigenvalues at $t = 63$ s.

to Geissler (1970), the maximum value of the natural frequency (of the controlled rigid body motion) should be less than one-fifth of the first bending-mode frequency, to keep the rigid and elastic modes separated. Moreover, Jerger and Merrill (1960) provides a rule of thumb to establish a lower bound. It thus follows that the closed-loop rigid-body requirement is 3 rad/s $\leq \omega_r \leq$ 8 rad/s, with a damping factor of $\zeta \approx 0.7$. Of course, the maximum natural frequency also depends on the physics of the system. The engine deflection angle as well as vehicle attitude and engine deflection rates should at all times remain beneath their limit values. By inspecting comparable launchers, it is established that a maximum engine deflection angle $-6° \leq \varepsilon_{T,max} \leq 6°$, a maximum engine deflection rate of $-100°/\text{s} \leq \dot{\varepsilon}_{T,max} \leq 100°/\text{s}$, and a maximum pitch rate of $-10°/\text{s} \leq q \leq 10°/\text{s}$.

From a root-locus analysis one finds that it is possible to stabilise the system for proportional-gain values larger than $K_p = 1.86$ (derivative gain $K_d = 0$). This proportional controller results in a slow response, which is also very oscillatory. The conclusion is that a non-zero K_d is required for a proper response. Further analysis shows that selecting $K_p = 4$ and $K_d = 1.2$ s yields a satisfactory response, with $\omega_{r,cl} = 4.7$ rad/s and $\zeta_{r,cl} = 0.83$, the latter of which is a bit larger than required, but this should not pose a problem. The unstable drift mode has also stabilised, with $\lambda_{3,cl}$ = -0.097.

When the servo dynamics are included in the analysis, three more poles are introduced (Fig. 5), where the periodic eigenvalues are due to the engine inertia, *i.e.,* the earlier mentioned *tail-wags-dog*. Despite the specification of $\omega_e = 50$ rad/s, the inclusion of

a non-unity torque feedback gain K_e, the natural frequency of the engine dynamics is only $\omega_e' = 36.3$ rad/s (with $\zeta_e = 0.57$). Adding the engine dynamics leads to an increase of the closed-loop rigid-body mode frequency to $\omega_{r,cl} = 9.4$ rad/s with a damping of $\zeta_{r,cl} = 0.73$. As $\omega_{r,cl}$ is too large now, K_p can be reduced to compensate for this. A further analysis leads to $K_p = 2.8$ and $K_d = 0.9$ s, with natural frequencies of $\omega_{r,cl} = 4.9$ rad/s (rigid body) and $\omega_{e,cl}$ 37.1 rad/s (engine), with damping factors $\zeta_{cl} = 0.75$ and $\zeta_e = 0.64$. As can be seen the engine has recovered some of its damping. The aperiodic rigid-body drift has become a bit more stable, with $\lambda_{3,cl}$ = -0.108.

In terms of gain and phase margins, the phase margin, P_m, for θ is infinite, whereas the gain margin, G_m, is 20.1 dB (at $\omega = 9.52$ rad/s), which has dropped down from infinity when just the rigid body was considered. This gain margin still guarantees sufficient stability. In Fig. 6, the Bode plots of α, θ and ε_T are shown. It can be seen that the frequency response of α and θ are almost identical. This can also be seen from the transient responses to a step function (not shown here). For input signals, *i.e.*, $\varepsilon_{T,c}$, with a frequency above 6 rad/s the dynamic gain decreases. The dip around 50 rad/s is due to the *tail-wags-dog* eigenvalue pair, which limits the amplitude at this frequency. The bandwidth of ε_T is somewhat larger and its response is less damped (gain margin of 13.2 dB at $\omega = 22.9$ rad/s, phase margin is 91.1°, at $\omega = 8.94$ rad/s), resulting in a small resonance peak at its natural frequency. Therefore, the stability and response of the rigid launcher with servo dynamics is acceptable.

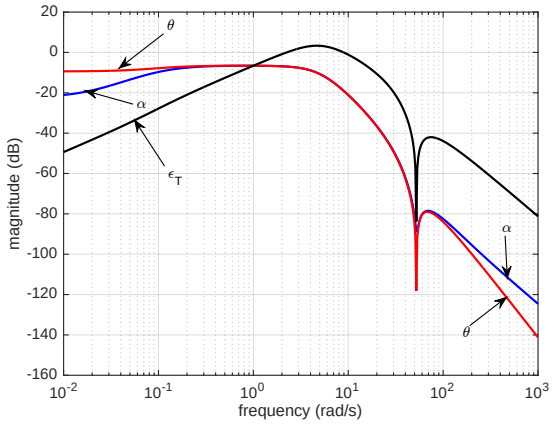

Fig. 6: Bode plot of attitude and engine angles

The effects of adding a single bending mode to the system are briefly examined, initially without structural damping ($\zeta_s = 0$), and then with the standard value of $\zeta_s = 0.015$. In both situations the controlled system parameters of $K_p = 2.8$ and $K_d = 0.9$ s are used. Adding the bending mode without structural damping leads to an additional pole pair ($\omega_{f1} = 42.2$ rad/s), which is unstable, albeit marginally ($\zeta_{f1} = -6.63 \cdot 10^{-4}$). It appears that there is no way of stabilising this mode for any value of K_p and K_d. With structural damping, the mode does become stable, with $\zeta_{f1} = 1.44 \cdot 10^{-2} \approx \zeta_s$. The bending mode (either damped or undamped) has a small effect on the rigid-body mode, its natural frequency slightly increases from $\omega_{r,cl} = 4.9$ rad/s to 5.1 rad/s. The damping increases from 0.75 to 0.76. The eigenmodes of the engine are hardly affected.

Now, include the higher bending modes, listed in Table 4: for four bending modes, there are, of course, four extra zero-pole pairs. All four are unstable, with damping factors of $\zeta_{f1} = -6.50 \cdot 10^{-4}$, $\zeta_{f2} = -1.50 \cdot 10^{-3}$, $\zeta_{f3} = -3.73 \cdot 10^{-4}$, and $\zeta_{f4} = -5.84 \cdot 10^{-4}$. It is obvious that the second bending mode is the most unstable. Adding structural damping changes the damping factors to $\zeta_{f1} = 1.44 \cdot 10^{-2}$, $\zeta_{f2} = 1.35 \cdot 10^{-2}$, $\zeta_{f3} = 1.46 \cdot 10^{-2}$, and $\zeta_{f4} = 1.44 \cdot 10^{-2}$, values close to the actual value of ζ_s.

The Bode plot for the elastic system is shown in Fig. 7, and shows that the elastic mode may pose a problem. It is clear that it will be amplified, while controlling an error in the pitch angle (by using the engine swivel angle), even at low frequencies. However, it should be noted that if the deformations remain small, the problems may remain limited. At its natural frequency, the bending mode spikes. In terms of gain and phase margins, the system has changed as follows. For α and θ, G_m and P_m have not changed. For the engine, though, the changes are significant: $G_m = 9.91$ dB (was 13.2 dB) at $\omega = 0.527$ (22.9) rad/s, P_m = -84.1° (91.1°), at $\omega = 3.51$ (8.94) rad/s. As the frequencies are low, this may interfere with the control. For the bending mode the gain and phase margins are G_m = -5.6 dB at $\omega = 0.53$ rad/s and $P_m = 71.7°$ at $\omega = 0.064$ rad/s. In the second part of this section we will look at the transient response, and how these gain and phase margins affect the controllability. This will be done for the structurally damped system.

Response Analysis

To study the transient response the perturbation con-

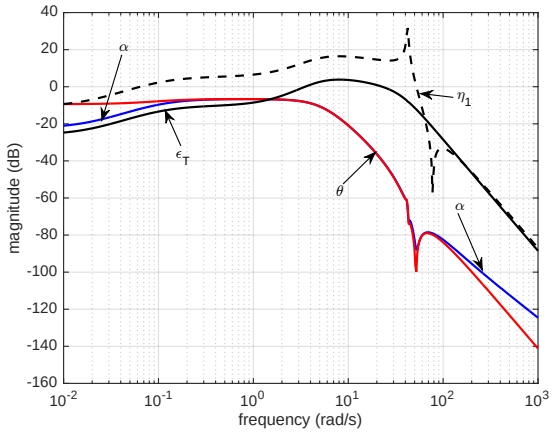

Fig. 7: Bode plot of attitude and engine angles, and first generalised coordinate

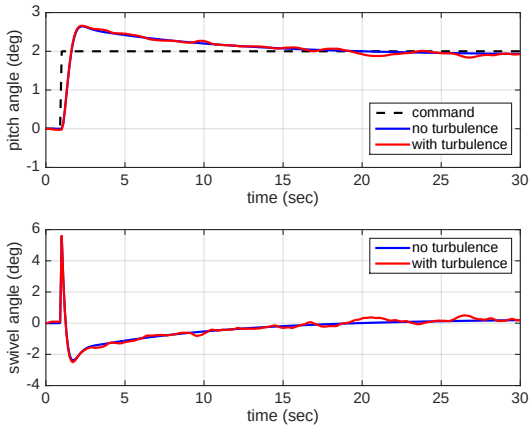

Fig. 8: Rigid-body response to a step-command of $\theta_c = 2°$, moderate turbulence

trol due to an offset in pitch angle of 1° is analysed. This is done for two conditions, one without wind and one with turbulence that affects the angle of attack. The turbulence is modelled with Dryden spectral densities, as a white noise passing through a linear, rational filter (DoD, 1980; Justus *et al.*, 1990). Parameters used are a scale length at medium/high altitudes of $L_w = 1100$ m, a gust intensity of $\sigma_w = 1.73$ m/s, and a probability of exceedance of high-altitude intensity of 10^{-3} (moderate conditions). The model is evaluated for an altitude of $h_0 = 11$ km and $u_0 = 493.07$ m/s, and will, in this case, produce a noisy wind component in the Z-direction, Δw. As before, this can be converted to an equivalent angle-of-attack perturbation of $\Delta\alpha_t = \frac{\Delta w}{u_0}$. This perturbation is added as a forcing function to the state-space model, by creating a second input and extending the input matrix $\mathbf{B}$ with a copy of the first column of $\mathbf{A}$ (the one associated with α). As such, the system will respond to $\Delta\alpha_t$ as it would to α.

Currently, it is desired only to illustrate the effect of modelling issues on the performance of a reasonably stable, closed-loop rigid-body launcher. Having said this, Fig. 8 shows the rigid-body response to a 2°-step in θ. The response is somewhat sluggish, and could, of course, be improved by increasing the gains. The response is stable, for both cases; however, the effect of encountering turbulence is visible. It is noted that perfect knowledge about the feedback states, θ and q, is assumed. The latter, in this case, is the rotation around the centre of mass, implying that a possible gyro would be located there. Later on, the effect of moving the gyro to a more logical location is considered.

For the next response analysis, the engine dynamics and the bending modes are included. Just adding the engine dynamics does not change the response of the system shown in Fig. 8, at least not noticeably. The engine dynamics are fast enough to track $\varepsilon_{T,c}$, although there is a small delay when the step is applied. However, the rigid-body response is decoupled from the engine response. The same actually applies when the bending modes are added. They are well separated from the rigid-body modes and are thus decoupled for this step response. Even for a severe turbulence ($L_w = 1100$ m and $\sigma_w = 6.0$ m/s), the system remains stable. This response is shown in Fig. 9: despite the angle-of-attack induced oscillations, the closed-loop system is well-behaved.

Adding the two slosh modes (Table 4) does not influence the transient response much, although an oscillation in the commanded swivel angle is introduced (Fig. 10) that also shows as an oscillation in the pitch angle, albeit the presence of turbulence seems to diminish this oscillation. It should be analysed in more detail how this oscillation affects the structure, in terms of loads and stresses, as well as the servo mechanism actuating the engine. Figure 11 shows the required actuation moments, which are calculated according to $M_e = I_e\ddot{\varepsilon}_T$. A spike is obviously observed when the step command is executed, which by itself should be checked for its feasibility. However, the noisy swivelling requires attention as the actuating moment is not negligible.

Concerning the deformation of the body, one may look at the deformation induced by each of the four

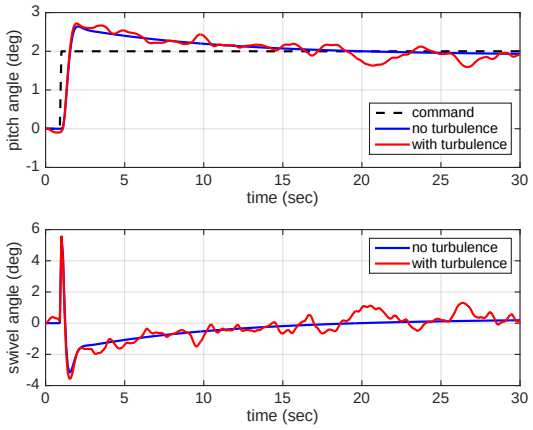

Fig. 9: Flexible-body response to a step-command of $\theta_c = 2°$, severe turbulence

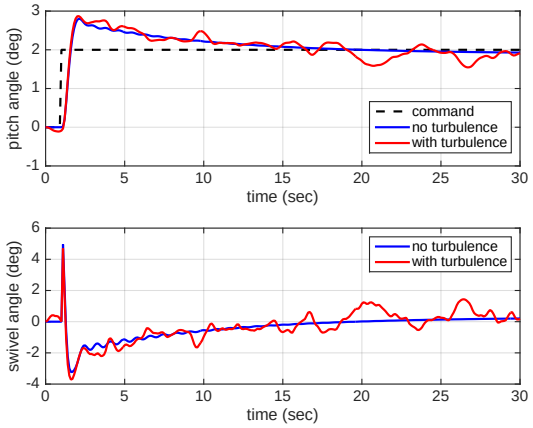

Fig. 10: Flexible-body response to a step-command of $\theta_c = 2°$, severe turbulence, with sloshing

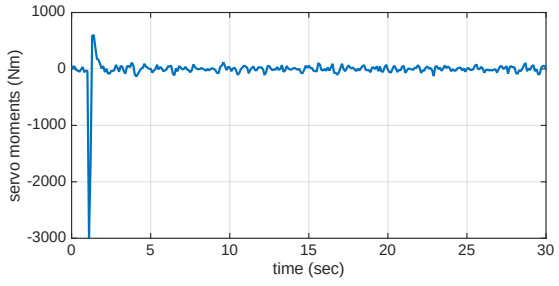

Fig. 11: Required engine actuation moments ($\theta_c = 2°$, severe turbulence, with sloshing)

flexible modes, Eq. [13]; the sloshing modes behave more or less like rigid-body modes and do not cause much deformation. The maximum deformation occurs at $t = 1.2$ s when the largest control effort takes place. In Fig. 12, this deformation is shown. The maximum difference is around 8 mm. It remains to be analysed what kind of stress this introduces in the structure.

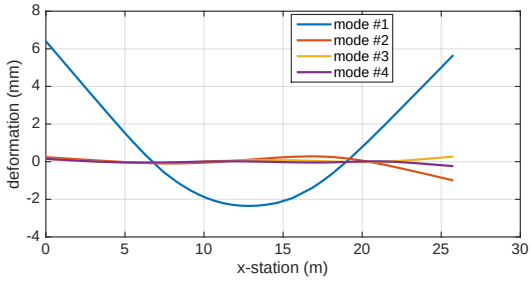

Fig. 12: Maximum deformation of the launcher at $t = 1.2$ s ($\theta_c = 2°$, severe turbulence, with sloshing)

So far it is assumed that the measurements of θ and q are ideal and known for the location of the centre of mass, and are not affected by the deformation of the launcher. In reality, the gyros also measure the deformation of the structure at the attachment point of the sensors. Usually, the gyros are placed at the forward end of the second stage, just below the payload adapter. For the PacAstro, this means that the gyros are placed at $x_{gyro} = 21.5$ m, so 9.5 m above the current centre-of-mass location ($x_{cm} = 12.0$ m). The gyro measurements, $\tilde{\theta}$ and $\tilde{q}$, are a combination of the rigid-body parameters and the angular displacement of the gyro's location due to flexibility:

$$\tilde{\theta} = \theta_r + \sum_{i=1}^{N} \sigma_i(x_{gyro})\eta_i \qquad [53]$$

$$\tilde{q} = q_r + \sum_{i=1}^{N} \sigma_i(x_{gyro})\dot{\eta}_i \qquad [54]$$

These are the signals that are fed back to the controller. The simulations will be done without turbulence and with moderate turbulence.

In Fig. 13, the response curves are shown for the flexible launcher without sloshing. In principle, the pitch-angle response looks to be convergent to 2°, but if one looks at the swivel angle he sees that it is oscillating severely, irrespective of turbulence being present. It is only due to the fast servo dynamics that the controller remains stable, being effectively a rapid bang-bang controller. Of course, the actual actuation power is not taken into account here, nor are

the vibrations and the structural loads it will induce. It is safe to conclude that the launcher cannot sustain this and will most likely break up. The measurements of the gyros are shown in Fig. 14. They confirm that the vibrations at the location of the gyros are severe. Note that, for comparison, the rigid-body equivalents are plotted as well.

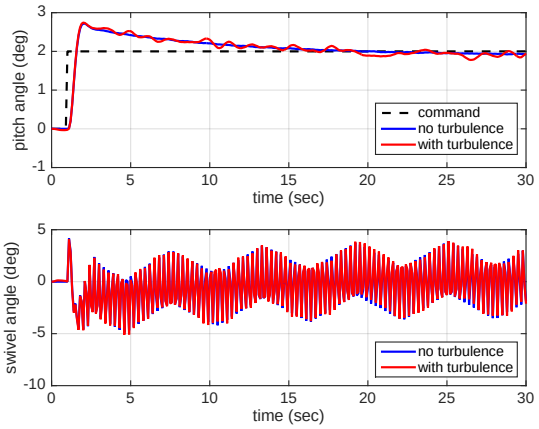

Fig. 13: Flexible-body response with gyro measurements ($\theta_c = 2°$, moderate turbulence)

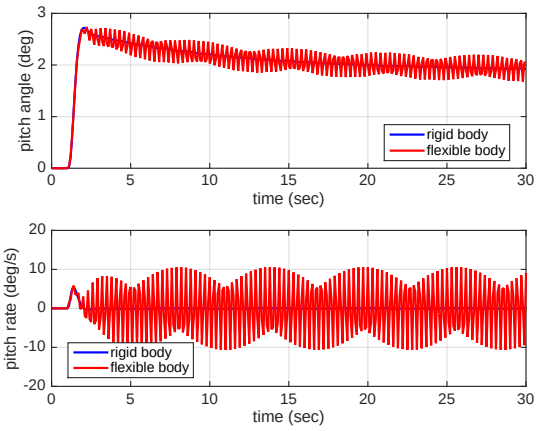

Fig. 14: Gyro measurements ($\theta_c = 2°$, moderate turbulence)

To complete the analysis, the result for the launcher with the sloshing modes is also included. It follows that the results are even worse than before. The plots are shown in Figs. 15 and 16. The controller is no longer capable of stabilizing the vehicle and the pitch angle diverges.

Therefore, it can be concluded that sensor placement and measurement filtering is important, but only in combination with a robust controller. If the sensor placement of a well-controlled system has no effect on its controllability, then sensor placement does not warrant any further study.

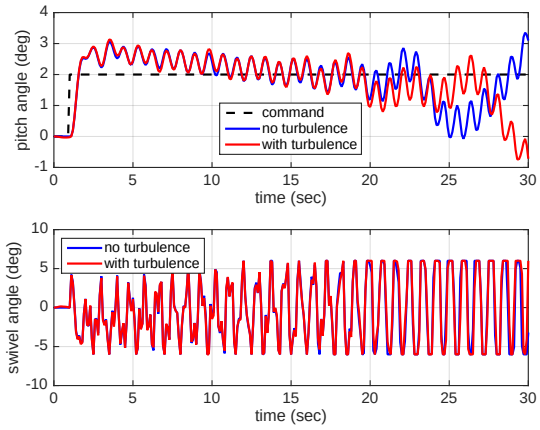

Fig. 15: Flexible-body response with gyro measurements ($\theta_c = 2°$, moderate turbulence, sloshing)

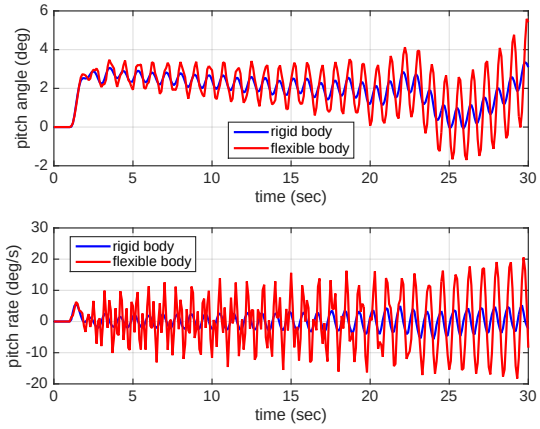

Fig. 16: Gyro measurements ($\theta_c = 2°$, moderate turbulence, sloshing)

VII. Conclusions

The bending modes and natural frequencies of the flexible launcher have been determined in NASTRAN. When sloshing is included, the eigenfrequencies of the flexible modes tend to slightly increase, but the appearance of low-frequency sloshing modes approach rigid-body-like modes. A root-locus analysis at one design point shows potential instability of the rigid body modes, but a non-zero proportional and derivative gain can stabilise the system. Including the bending modes has a destabilising ef-

fect on the system, however, it can be compensated with industry-standard structural damping. The response due to turbulence, swivel-engine control inputs, sloshing, and gyro placement are also simulated for 2° step-commands. The step response of a flexible launcher without sloshing seems to be convergent, regardless of the turbulence, but a closer look at the engine swivel angle shows that it is effectively at the limit of control, and including sloshing worsens the situation and the pitch angle diverges.

This research focussed on the point during the flight of maximum dynamic pressure, which occurs at $t = 63\ s$. Although this is considered to be the worst-case control point in the path, ideally the entire flight path stability and control should be considered, focussing on the effects of continuously reducing the fuel and oxidiser volume over the duration of flight.

References

Capri, F., Mastroddi, F. and Pizzicaroli, A., "Linearized Aeroelastic Analysis for a Launch Vehicle in Transonic Flight Conditions", *Journal of Spacecraft and Rockets*, Vol. 43, No. 1, 2006, pp. 92-104.

Craig, Jr., R.R., *Structural Dynamics. An Introduction to Computer Methods*, John Wiley & Sons, New York, 1981.

Department of Defense, "Flying Qualities of Piloted Airplanes", MIL-F-8785C, Nov. 5, 1980.

Ebrahimian, M., Noorian, M.A. and Haddadpour, H., "Equivalent Mechanical Model of Liquid Sloshing in Multi-Baffled Containers", *Engineering Analysis with Boundary Elements*, Vol. 47, 2014, pp. 82-95.

Etkin, B. and Reid, L.D., *Dynamics of Flight. Stability and Control*, 3^{rd} Edition, John Wiley & Sons, Inc, 1996.

ESDU, "Normal-force-curve and pitching-moment-curve slopes of forebody-cylinder combinations at zero angle of attack for Mach numbers up to 5", ESDU 89008, with Amendments A and C, December 1990.

Fleeter, R., Mcloughlin, F. and Mills, R., "A Low-Cost Expendable Launch Vehicle for 500-Pound Class Satellites", Marketing brochure, PacAstro, Herndon, VA, 26 May 1992.

Foist, B.L., Grau, E.L., Nejad, B.I., "Launch Loads Development Using Sine Vibration Methodology", AIAA-20041800, *45^{th} AIAA/ASME/ASCE/AHS/ASC Structures, Structural Dynamics & Materials Conference*, Palm Springs, California, 19-22 April 2004.

Geissler, E.D., "Wind Effects on Launch Vehicles", AGARDograph No. 115, 1970.

Ibrahim, R.A., *Liquid Sloshing Dynamics. Theory and Applications*, Cambridge University Press, 2005.

Junkins, J.L. and Kim, Y., *Introduction to Dynamics and Control of Flexible Structures*, AIAA Education Series, American Institute of Aeronautics and Astronautics, Reston, VA, 1993.

Jerger, J.J. and Merrill, G., *Systems Preliminary Design*, Van Nostrand, Princeton, N.J., 1960.

Justus, C.G., Campbell, C.W., Doubleday, M.K., and Johnson, D.L., "New Atmospheric Turbulence Model for Shuttle Applications", NASA TM-4168, January 1990.

Lester, H.C. and Collins, D.F., "Determination of Launch-Vehicle Response to Detailed Wind Profiles", AIAA-64-82, *Aerospace Sciences Meeting*, New York, NY, 1964.

Li, M., Rui, X. and Abbas, L.K., "Elastic Dynamic Effects on the Trajectory of a Flexible Launch Vehicle", *Journal of Spacecraft and Rockets*, Vol. 52, No. 6, 2015, pp. 1586-1602.

Meirovitch, L., and Wesley, D. A., "On the Dynamic Characteristics of a Variable-Mass Slender Elastic Body Under High Accelerations", *AIAA Journal*, Vol. 5, No. 8, 1967, pp. 1439-1447.

Nichkawde, C., Harish, P.M. and Ananthkrishnan, N., "Stability Analysis of a Multibody System Model for Coupled Slosh-Vehicle Dynamics", *Journal of Sound and Vibration*, Vol. 275, 2004, pp. 1069-1083.

Nielsen, J.N., *Missile Aerodynamics*, New York: McGraw-Hill, 1960.

Noorian, M.A., Haddadpour, H. and Ebrahimian, M., "Stability analysis of elastic launch vehicles with fuel sloshing in planar flight using a BEM-FEM mode", *Aerospace Science and Technology*, Vol. 53, 2016, pp. 74-84.

Orr, J.S., "A Coupled Aeroelastic Model for Launch Vehicle Stability Analysis", AIAA-2010-7642, *AIAA Atmospheric Flight Mechanics Conference*, Toronto, Canada, 2-5 August 2010.

Orr, J.S., Johnson, M.D., Wetherbee, J.D., and McDuffie, J.H., "State Space Implementation of Linear Perturbation Dynamics Equations for Flexible Launch Vehicles", AIAA 2009-5962, *AIAA Guidance, Navigation, and Control Conference*, Chicago, IL, 10-13 August 2009.

Platus, D.A., "Aeroelastic Stability of Slender, Spinning Missiles", *Journal of Guidance, Control, Dynamics*, Vol.15., No. 1, 1992, pp. 144-151.

Rolland Collette, J.G., "Analysis and Design of Space Vehicle Flight Control Sytems, Volume XI, Component Dynamics", NASA CR-830, 1967.

Schwanz, R.C. and Cerra, J.J., "Dynamic modeling uncertainty affecting control system design", AIAA-84-1057, From: *AIAA Dynamics Specialists Conference*, Palm Springs, CA, May 17-18, 1984.

Seifert, H.S. and Brown, K., *Ballistic Missile and Space Vehicle Systems*, New York: John Wiley & Sons, 1961

U.S. Army Materiel Command, "Engineering Design Handbook. Liquid Filled Projectile Design", AMC Pamphlet Nr. 706-165, April 1969.

Yang, H.Q. and Peugeot, J., "Propellant Sloshing Parameter Extraction from Computational-Fluid-Dynamics Analysis", *Journal of Spacecraft and Rockets*, Vol. 51, No. 3, 2014, pp. 908-916.